JMEPEG (2020) 29:1–9
https://doi.org/10.1007/s11665-019-04524-y

1059-9495/$19.00

Mechanical and Electrical Properties and Phase Analysis of Aged Cu-Mg-Ce Alloy

Junchao An, Bingjie Wang, Yi Zhang, Baohong Tian, Alex A. Volinsky, Yong Liu, and Guangxin Wang

(Submitted April 11, 2019; in revised form November 24, 2019; published online December 23, 2019)

Aging behavior of the Cu-Mg-Ce alloy of various cold deformations with aging temperature ranging from 400 to 480 °C and aging time ranging from 10 to 480 min was investigated. Effects of the secondary phase on hardness and electrical conductivity were discussed. Electrical conductivity and phase transformation kinetics equations were established. The addition of Ce promoted the precipitation of the secondary phase, improved the hardness, and delayed the dynamic recrystallization of the Cu-Mg alloy in the aging process. Nanoscale secondary phases in the aging process were determined to be α-Fe and Mg_3P_2. α-Fe particles lead to dispersion strengthening and the peak-aging stage. The Mg_3P_2 particles play an important role in inhibiting the motion of grain boundaries and the precipitation of coarse Fe_2P or Fe_3P. The secondary phases α-Fe and Mg_3P_2 pinned at dislocations and twin boundaries improved the softening resistance of the Cu-Mg-Ce alloy. Optimal aging parameters of the Cu-Mg-Ce alloy are 60% cold deformation aged at 420 °C for 20 min with 205.82 HV hardness, 73.59%IACS electrical conductivity, 597 MPa ultimate tensile strength, and 4.39% elongation.

Keywords aging behavior, cold deformation, Cu-Mg-Ce alloy, hardness, nanoscale particles

1. Introduction

Due to the high strength and excellent conductivity, copper alloys are widely used as electronic connectors, electrical contact wires and lead frame materials (Ref 1-3). With the rapid development of the high-speed railways, the study of high-performance copper-electric contact wire attracts the attention of many researchers. Cu-Mg alloy electric contact wire is widely used in high-speed railway with over 350 km/h speed (Ref 4-6). Therefore, excellent tensile strength, high elongation and high thermal stability are required. Numerous investigations have focused on the equal channel angular pressing (ECAP), high-pressure torsion (HPT), and cold rolling to obtain superior properties. However, the above methods mainly emphasize the deformation behavior. Besides, these methods are complicated, have low production efficiency and produce limited size products.

Precipitation strengthening is an effective method for strengthening alloys. Typical precipitation-hardened alloys are Cu-Cr-Zr, Cu-Ni-Si, and Cu-Fe-P (Ref 7-9). Mu et al. (Ref 10) confirmed that the Cu-Cr-Zr-Mg-RE alloy has a good combination of physical and mechanical properties through precipitation of multiple phases: chromium-rich phase, zirconium-rich phase, and the $CrCu_2$ particles. Lee et al. (Ref 11) proved that the NiSi phase nanoscale precipitates enhanced the tensile strength and elongation of the Cu-Ni-Si alloy during aging. Liu et al. (Ref 12) found that the secondary phase inhibits recrystallization during the aging treatment of the Cu-Cr-Zr-Mg alloy. The combination of solid solution and aging treatment is an important way to achieve dispersion strengthening. It has been proven that the Fe element delays the recrystallization process of copper and improves its strength and hardness. P element improves the mechanical properties and weldability of copper alloys. In addition, it is well known that the rare earth elements can refine the matrix microstructure and eliminate the influence of impurity elements. Guo et al. (Ref 13) proved that the addition of Ce could facilitate the precipitation of the strengthening phases in the Cu-Fe-P-Cr alloy. Wang et al. (Ref 14) added trace Ce into the Cu-Mg alloy and found that Ce improved the high-temperature stability of the material. Lu et al. (Ref 15) investigated the effects of Ce addition on the Cu-Al-Mn alloy and proved that Ce doping refines the grains and causes the formation of the Ce-rich phase. Zhang et al. (Ref 16) confirmed that Ce addition can clean the grain boundaries and increase the nucleation rate of the precipitates in the aging process of the Cu-Cr-Zr alloy.

According to the above research, Fe, P and rare earth Ce element were added to the Cu-Mg alloy by vacuum melting. In this experiment, the main purpose of adding Fe and P is to form the Mg_3P_2 secondary phase and improve the mechanical properties of the alloy by dispersion strengthening. The aim of this work is mainly to investigate the properties and perform phase analysis of the Cu-Mg alloy in the aging process. The evolution of precipitates and their effects on the hardness and electrical conductivity of the alloy during aging were studied. Phase transformation kinetics and conductivity equations were established. The effects of Ce rare earth element on the alloy properties were investigated. In order to provide a theoretical

Junchao An, Luoyang Institute of Science and Technology, Luoyang 471023, People's Republic of China; **Bingjie Wang, Yi Zhang, Baohong Tian, Yong Liu,** and **Guangxin Wang**, School of Materials Science and Engineering, Henan University of Science and Technology, Luoyang 471023, People's Republic of China; and Collaborative Innovation Center of Nonferrous Metals, Luoyang 471023 Henan Province, People's Republic of China; and **Alex A. Volinsky**, Department of Mechanical Engineering, University of South Florida, Tampa 33620. Contact e-mails: superjun@tju.edu.cn, lywbj126@126.com, zhshgu436@163.com, and tianbh@haust.edu.cn.

basis for industrialized production, the optimal aging process parameters were determined.

2. Experimental Procedure

The raw materials for the test are pure Cu, pure Mg, pure Ce, Cu-10%Fe master alloy, and Cu-12%P master alloy with the total weight of 8 ± 0.5 kg. They were cast in the ZG-0.01 vacuum medium frequency induction melting furnace in a graphite crucible in argon at 1200 ± 10 °C. At the end of smelting, the solution was poured into a low-carbon steel mold with ϕ85 mm × 120 mm dimensions. Subsequently, the ingots were cooled to room temperature. Because the composition of the riser is not uniform and there are many impurities in the melting process, the riser part of the ingot was cut off. In order to eliminate dendrite segregation after smelting, homogenization annealing was carried out by the box-type resistance furnace (KSS-1200) heated at 900 °C for 2 h. Then the ingots were extruded into the cylinder with ϕ33 mm diameter by using the XJ-500 metal profile extrusion machine. After the solution treatment at 900 °C for 2 h, the cylinder was processed into the 100 mm × 5 mm × 1 mm sheet. Subsequently, after various cold deformation of 40 and 60%, the specimens were aged at 400-480 °C for 10-480 min. Hardness at various conditions was measured by the HVS-1000 A hardness tester. Each specimen was measured 10 times to obtain an average value with the ± 5% measurement error. Electrical conductivity was tested by the ZY9987 digital micro-ohmmeter within ± 5% measurement error. Tensile properties were measured using the AG-I 250 KN machine. Three tension specimens under the same test conditions were prepared and tested separately. The error was less than ± 3%. The specimen for transmission electron microscopy (TEM) analysis was 50 mm thick with 3 mm diameter. It was thinned by using the Gatan 691 ion beam thinner with an incident angle of 9° and 5 keV ion beam energy. After the small holes appeared on the surface of the sample, the parameters were adjusted to 9° and 5 keV immediately, and then ion thinning continued for 30 min. Secondary phases formed in the aging process were analyzed by the transmission electron microscope (JEM-2100). Alloy composition analysis is listed in Table 1.

3. Results

3.1 Hardness and Electrical Conductivity

Figure 1(a) shows the variation of the hardness with aging time for the Cu-Mg-Ce alloy without cold deformation. The hardness increases rapidly in the initial stage and then decreases gradually after reaching the peak value. It is related to the precipitation of the secondary phases during the aging process (Ref 16, 17). In the early stage of aging, the precipitation rate of the secondary phases increased fast and caused dispersion strengthening. Subsequently, the secondary phases continued to precipitate, which hindered dislocation motion by in situ pinning. Therefore, the hardness continued to rise until it reached the peak value. Subsequently, with the continued aging process and larger precipitates, the over-aging stage appeared, leading to the hardness decrease. It is notable that the Cu-Mg-Ce alloy has the maximum hardness aging at 420 °C and the obvious over-aging phenomenon occurs when the temperature is higher than 420 °C, i.e., 440, 460, and 480 °C. The reason is that the secondary phase has a higher growth rate at high temperature, which leads to the weakness of the interaction between the secondary phase and the matrix. As a result, it reduced the strengthening effects (Ref 18). For instance, the hardness of the Cu-Mg-Ce alloy at the peak stage at various aging temperatures of 400, 420, 440, 460, and 480 °C are 150.14, 168.36, 168.20, 160.58, and 156.33 HV, respectively.

Table 1 Chemical composition of the Cu-Mg-Ce alloy

	Analyzed composition, wt.%			
Nominal composition, wt.%	**Mg**	**Fe**	**P**	**Ce**
Cu-0.4Mg-0.2Fe-0.15P	0.406	0.194	0.151	…
Cu-0.4Mg-0.2Fe-0.15P-0.15Ce	0.395	0.189	0.146	0.153

The precipitation and growth of the secondary phase also have a significant effect on the electrical conductivity of the alloy. Figure 1(b) shows the variation of the electrical conductivity of the Cu-Mg-Ce alloy with aging time and temperature. In the early stage of aging, the precipitation of the secondary phase purifies the matrix, the scattering effects of alloying elements on electrons are reduced, and thus the conductivity rises rapidly (Ref 19, 20). The higher the temperature, the faster the precipitation rate. Subsequently, the precipitation rate of the secondary phase decreases with aging time and the conductivity increases slowly. Finally, the secondary phase completely precipitated from the matrix, and the conductivity remained stable. Figure 1(c) shows the variation of the hardness with aging time and different cold deformations of the Cu-Mg-Ce alloy aged at 420 °C. The hardness of the alloy after 0, 40, and 60% cold deformation without aging treatment are 105.6, 145.3, and 150.6 HV, respectively. The Cu-Mg-Ce alloy has the maximum hardness after 60% cold deformation in the aging process. The reason is that larger cold deformation caused more lattice distortion, which leads to greater hindrance of dislocations movement. As a result, the orientation of crystals can only be changed by twinning in the matrix and furthermore promoted slipping (Ref 21-23).

The appearance of twins reduces the average free path of dislocations and plays an important role in strengthening. Besides, many twins cause an increase in grain boundaries, which indicates the increased width of extended dislocations (Ref 14). Therefore, the movement of dislocations is further hindered and the hardness increases. As seen in Fig. 1(d) for the Cu-Mg-Ce alloy aged at 420 °C, the electrical conductivity increased with cold deformation. The reason is that larger cold deformation caused more vacancies and dislocations in the matrix, which is beneficial for the precipitation of the secondary phase in the subsequent aging process (Ref 24). Based on the above phenomena, the optimal aging parameters for the Cu-Mg-Ce alloy are 60% cold deformation with 420 °C aging for 20 min. The hardness is 205.82 HV, and electrical conductivity is 73.59%IACS. These phenomena can be further studied by analyzing the microstructure by TEM.

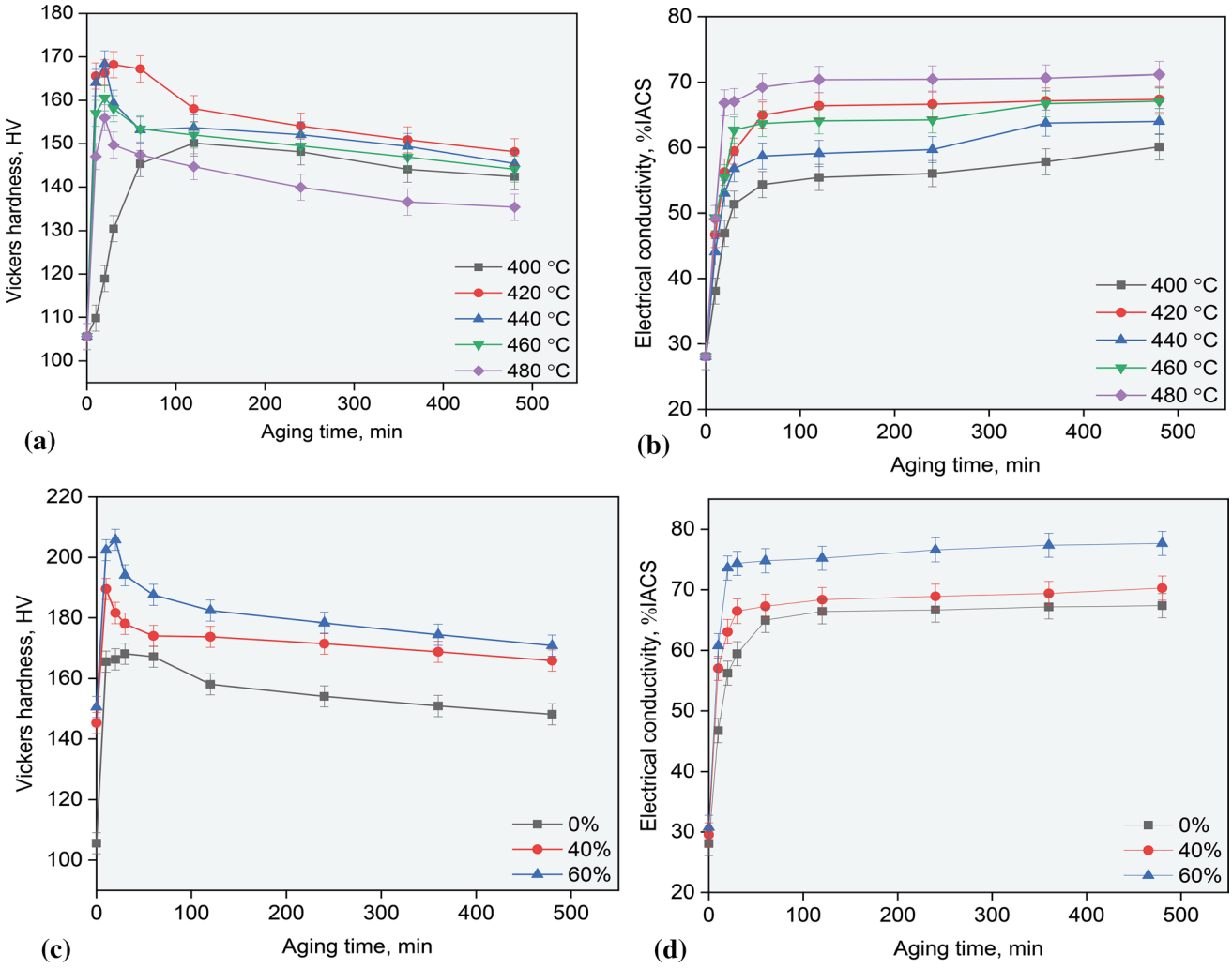

Fig. 1 Variation of (a, c) Vickers hardness and (b, d) electrical conductivity of the Cu-Mg-Ce alloy after (a, b) 0% and (c, d) 60% cold deformation aged at 420 °C

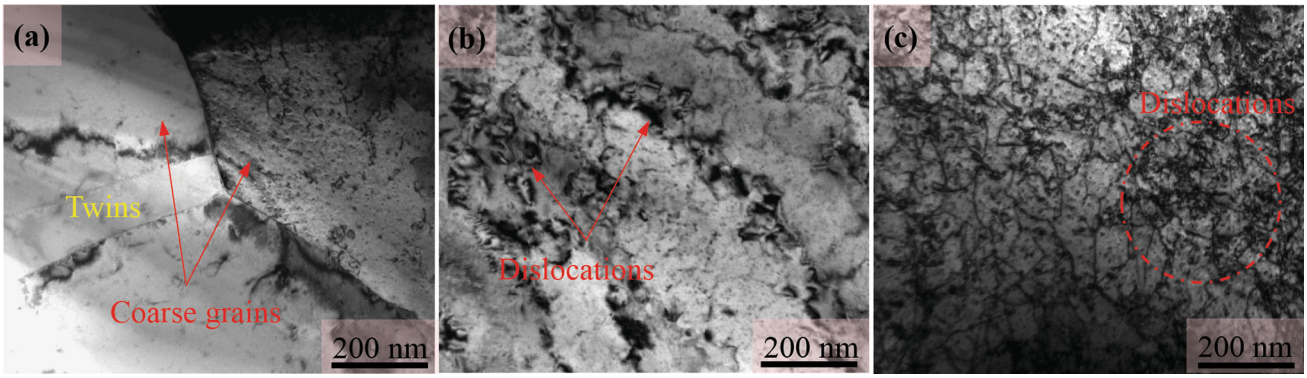

Fig. 2 TEM images of the Cu-Mg-Ce alloy after (a) 40% cold deformation and (b) 60% cold deformation

3.2 TEM Observations

The TEM image of the Cu-Mg-Ce alloy without cold deformation is shown in Fig. 2(a), where the matrix consists of mainly coarse grains and annealing twins. TEM images of the Cu-Mg-Ce alloy after 40 and 60% cold deformation are shown in Fig. 2(b) and (c), respectively. Compared with Fig. 2(a), many high-density dislocations appeared in the 40 and 60% deformed alloy matrix. In addition, the alloy matrix with 60% cold deformation has the highest dislocation density. The dislocations tangled with each other and lead to the stress concentration (Ref 25-27). Therefore, the hardness of the alloy increases with deformation. The TEM images of the Cu-Mg-Ce alloy with 60% cold deformation aged at 420 °C for 20 min are shown in Fig. 3(a). Numerous ultrafine precipitates are uni-

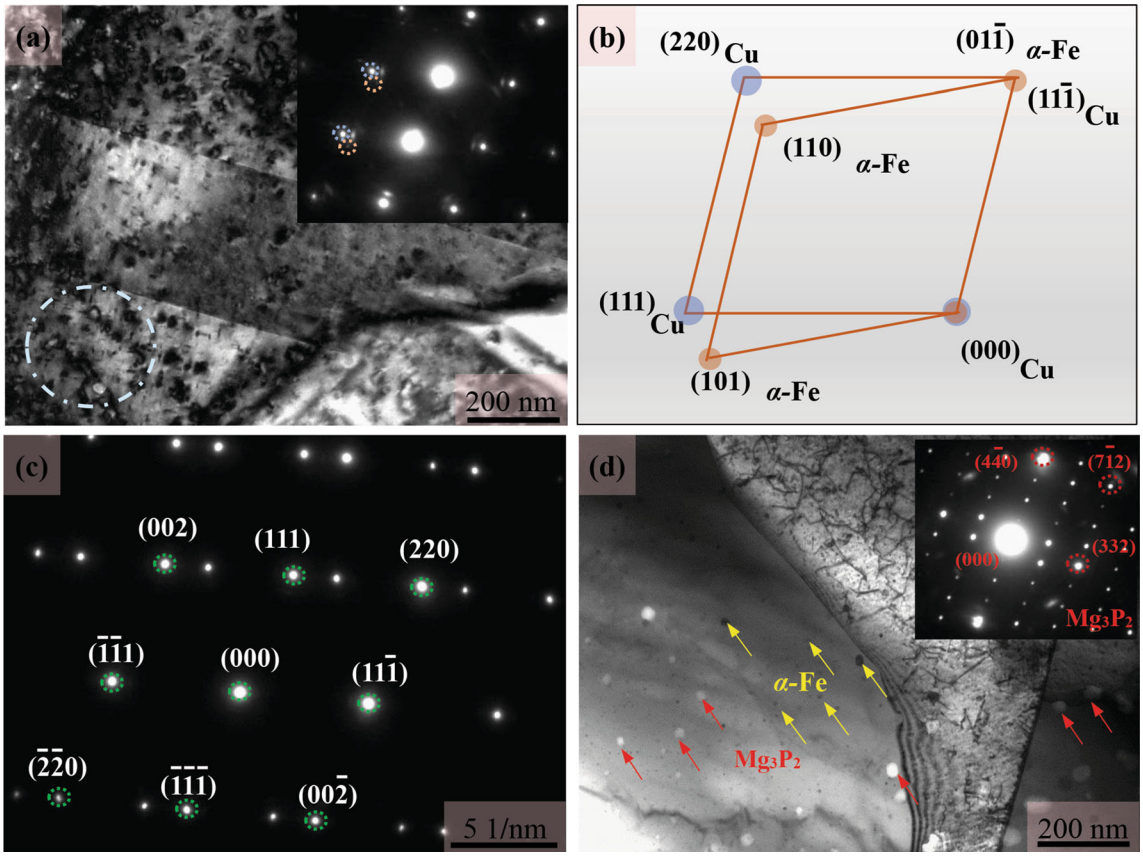

Fig. 3 TEM images of the Cu-Mg-Ce alloy with 60% cold deformation aged at 420 °C (a) bright-field image after 20 min aging; (b) SAED pattern of selected secondary phase in (a); (c) SAED pattern of twin structure in (a); (d) bright-field image after 240 min aging

formly distributed in the matrix. Thus, the enhanced hardness at the peak-aging stage can be attributed to the precipitates. As seen in Fig. 3(b), the precipitates in Fig. 3(a) are nanoscale α-Fe. In addition, twins appeared in the matrix due to plastic deformation, and the corresponding crystal structure of the twins is shown in Fig. 3(c). The appearance of twins increased the number of grain boundaries and the resistance to dislocation movement. Figure 3(d) illustrates the TEM image of the Cu-Mg-Ce alloy aged for 240 min. The dislocation density decreased significantly, which lead to the stress release. However, there are still a few precipitates pinning the dislocations. Compared with the 20 min aging time in Fig. 3(a), the precipitates size under this condition is larger. The larger precipitates weaken the effects of dispersion strengthening. As a result, the phenomenon of over-aging occurs and the hardness of the alloy decreases.

It is worth mentioning that there are two types of secondary phases in Fig. 3(d). One type is α-Fe marked by the yellow arrow, and the other type marked by the red arrow is face-centered cubic Mg_3P_2. At present, there are a few reports of the Mg_3P_2 phase. Wang et al. (Ref 28) observed Cu_2Mg in the Cu-Mg alloy matrix after hot deformation. Kim et al. (Ref 29) confirmed coarse Fe_3P phase in the aged Cu-Fe-P alloy. However, there is no Fe_2P or Fe_3P in this condition, which indicates that the appearance of Mg_3P_2 hindered the precipitation of the coarse Fe_2P and Fe_3P phases. Therefore, the comprehensive properties of the alloy were optimized. The TEM images of the Cu-Mg alloy with 60% cold deformation aged at 420 °C for 240 min are shown in Fig. 4. As seen in Fig. 4(a), coarse precipitates pinned in the grain boundaries. Figure 4(b) shows the corresponding selective diffraction pattern. The precipitate is determined to be Fe_3P. This fully illustrated that the Ce addition to the Cu-Mg alloy promoted the precipitation of the Mg_3P_2 particles. Meanwhile, the precipitation of Mg_3P_2 inhibited the precipitation of Fe_2P and Fe_3P.

3.3 Kinetics of Precipitates Transformation of the Cu-Mg-Ce Alloy

In order to determine the effects of precipitation rate of the secondary phase on hardness and electrical conductivity of the Cu-Mg-Ce alloy in the aging process by the quantitative analysis, the equations of phase transformation kinetics were established to calculate the precipitation rate at a given aging stage by using the Origin 2018 software.

The precipitation rate (f) is defined as the ratio of the secondary phase volume at a certain stage (V) to the volume of the secondary phase (V_c) at the end of the aging process (Ref 30):

$$f = \frac{V}{V_c} \times 100\% \quad \text{(Eq 1)}$$

Here, no precipitates were observed before aging. Therefore, $V = 0$ and $f = 0$. At the end of the aging process, the secondary phase completely precipitated from the matrix, $V = V_c$ and $f = 1$. At this time, the alloy has the maximum conductivity. According to the Matthiessen's theory (Ref 31), the relationship

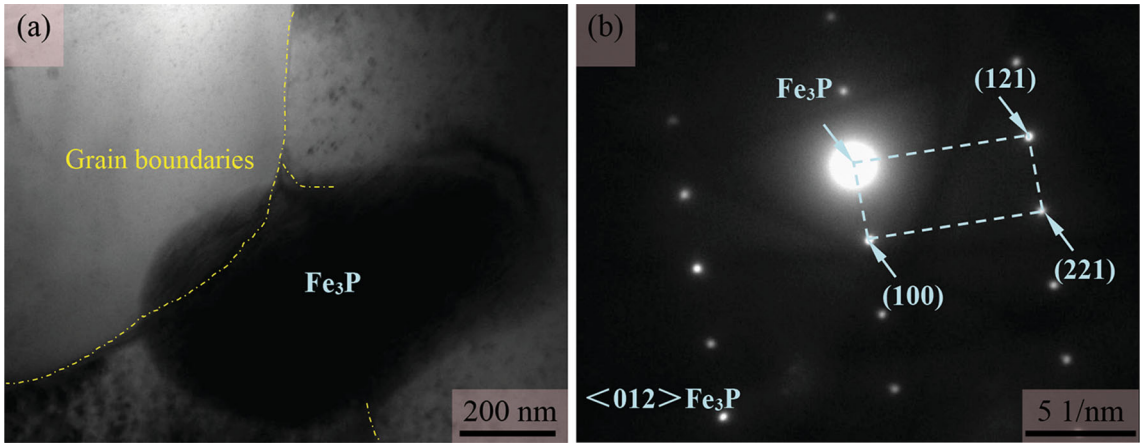

Fig. 4 TEM images of the Cu-Mg alloy with 60% cold deformation aged at 420 °C for 240 min (a) bright-field image; (b) SAED pattern of the secondary phase in (a)

between the electrical conductivity and precipitation rate can be determined as:

$$\gamma = \gamma_0 + Af \quad \text{(Eq 2)}$$

Here, γ is the electrical conductivity at the given aging stage; γ_0 is the electrical conductivity before aging; A is the parameter when conductivity reaches its maximum at $f = 1$. Therefore, the parameter $A = \gamma_{max} - \gamma_0$. This indicates that the precipitation rate of the secondary phase can be calculated by measuring the electrical conductivity of each aging stage.

Based on the Avrami equation (Ref 32), the relationship between the precipitation rate of the secondary phase and aging time is expressed as follows:

$$f = 1 - \exp(-bt^n) \quad \text{(Eq 3)}$$

Here, n and b are constants related to the type of phase transition, temperature and atomic size. Taking the logarithms of both sides of Eq 3 yields:

$$\lg\left(\ln\frac{1}{1-f}\right) = \lg b + n\lg t \quad \text{(Eq 4)}$$

According to the variation of conductivity of the Cu-Mg-Ce alloy with 60% cold deformation in Fig. 5(a), the $\lg[\ln(1/(1-f)] - \lg t$ curves are obtained in Fig. 5(b). The values of the slope n and intercept $\lg b$ are obtained, respectively. The value of n, b, and the electrical conductivity equations of various aging time and temperature are listed in Table 2.

The phase transformation kinetics curves of various aging temperature and time are shown in Fig. 5(c). The phase transformation kinetics curves have a smaller slope in the early aging stage. At the peak-aging stage, the precipitation rate increases rapidly. Then, after aging for 60 min, the slope is close to zero, which indicates that the volume fraction of precipitates is almost unchanged. As a result, the electrical conductivity of the alloy tends to be stable. The corresponding phase transformation kinetics equations can be expressed as follows:

$$\begin{bmatrix} f_{400\,^\circ C} = 1 - \exp(-1.321t^{0.615}) \\ f_{420\,^\circ C} = 1 - \exp(-2.661t^{0.335}) \\ f_{440\,^\circ C} = 1 - \exp(-2.761t^{0.334}) \\ f_{460\,^\circ C} = 1 - \exp(-3.329t^{0.274}) \\ f_{480\,^\circ C} = 1 - \exp(-1.531t^{0.482}) \end{bmatrix} \quad \text{(Eq 5)}$$

4. Discussion

4.1 Effects of Ce Addition on the Aged Cu-Mg Alloy

Previous studies have shown that rare earth elements can promote the secondary phase precipitation (Ref 14, 33, 34). Therefore, the TEM images of Cu-Mg and Cu-Mg-Ce alloys after 60% cold deformation aged at 420 °C for 480 min were obtained. As shown in Fig. 6(a), due to the long aging time, coarse grains appear in the matrix of the Cu-Mg alloy marked as A, B, C, and D with the average size of 2.95 μm. Meanwhile, there is only a small amount of precipitation in the matrix marked with the yellow circle. However, the TEM image of the Cu-Mg-Ce alloy in Fig. 6(b) shows that the number of precipitates in the Cu-Mg-Ce alloy is obviously higher than in the Cu-Mg alloy. The precipitates are pinned at dislocations and twin boundaries. This indicates that the twins produced by cold deformation are kept in the matrix and dynamic recrystallization is inhibited (Ref 35, 36). As a result, softening resistance of the Cu-Mg-Ce alloy is improved (Ref 37). The magnified image of the selected area is presented in Fig. 6(c). It can be clearly seen that the secondary phase is pinning the dislocation network and inhibits the dislocation movement. Therefore, the hardness of the Cu-Mg-Ce alloy increased.

The variation of hardness and electrical conductivity with the aging time of the Cu-Mg and Cu-Mg-Ce alloy aged at 420 °C with 60% cold deformation is shown in Fig. 7(a) and (b), respectively. For the Cu-Mg-Ce alloy, it takes 20 min to reach the peak-aging stage, while the Cu-Mg alloy needs 60 min. This also indicates that the Ce addition improves the softening resistance of the Cu-Mg alloy. The peak values of the Cu-Mg-Ce and Cu-Mg alloys hardness are 205.82 and 168.52 HV, respectively. The addition of Ce improved the hardness of the Cu-Mg alloy by about 22%. In addition, as shown in Fig. 7(b), the electrical conductivity of the Cu-Mg-Ce alloy is higher than the Cu-Mg alloy. At the peak-aging stage of hardness, the corresponding electrical conductivity of the Cu-Mg-Ce and Cu-Mg alloys is 74.36%IACS and 65.72%IACS, respectively. The addition of Ce improved the hardness of the Cu-Mg alloy by about 9%. Precipitation of Mg_3P_2 purified the alloy matrix, reduced the scattering of Mg and P atoms on

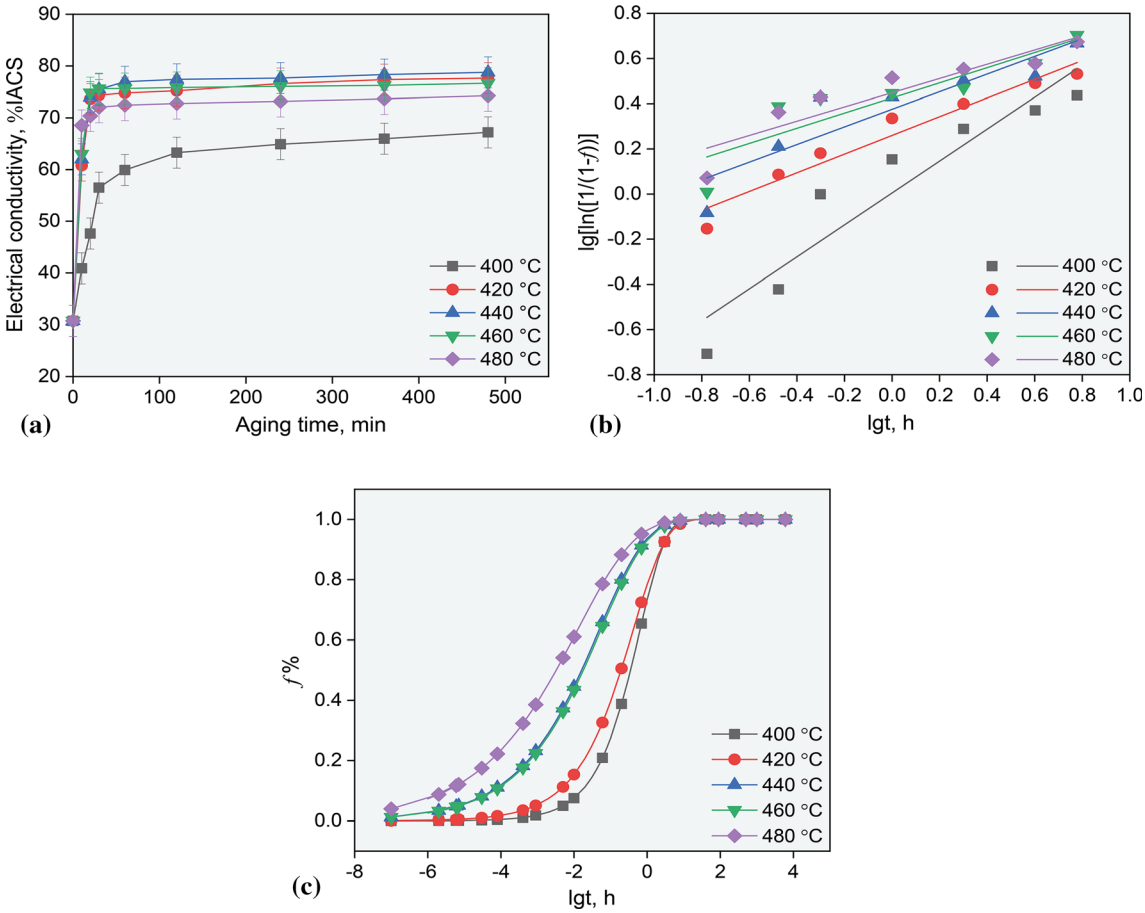

Fig. 5 Cu-Mg-Ce alloy with 60% cold deformation and various aging temperatures: (a) electrical conductivity curves; (b) lg[ln(1/(1 − *f*)] − lg*t* curves; (c) phase transformation kinetics curves

Table 2 Values of *n*, *b* and electrical conductivity equations of the Cu-Mg-Ce alloy

Temperature, °C	*n*	*b*	Phase transformation kinetics equations
400	0.615	1.321	$f_{400\,^\circ C} = 1 - \exp(-1.321t^{0.615})$
420	0.335	2.661	$f_{420\,^\circ C} = 1 - \exp(-2.661t^{0.335})$
440	0.334	2.761	$f_{440\,^\circ C} = 1 - \exp(-2.761t^{0.334})$
460	0.274	3.329	$f_{460\,^\circ C} = 1 - \exp(-3.329t^{0.274})$
480	0.482	1.531	$f_{480\,^\circ C} = 1 - \exp(-1.531t^{0.482})$

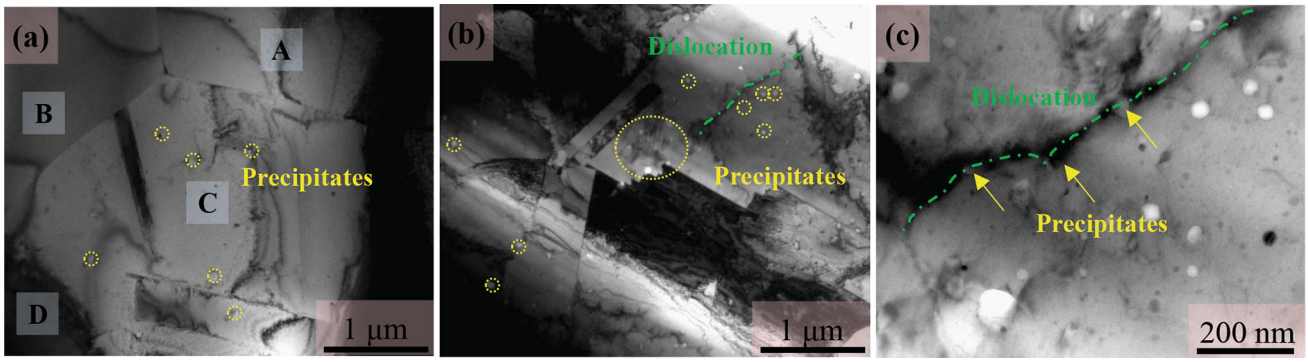

Fig. 6 TEM images of the Cu-Mg and Cu-Mg-Ce alloys after 60% cold deformation aged at 420 °C for 480 min: (a) Cu-Mg alloy; (b) Cu-Mg-Ce alloy; (c) magnification of the selected area in (b)

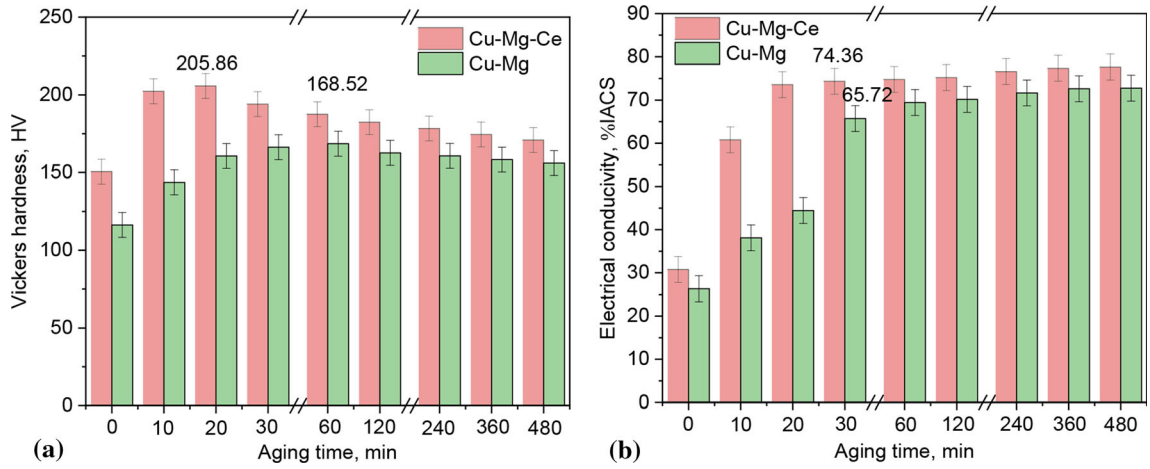

Fig. 7 Variation of hardness and electrical conductivity with the aging time of the Cu-Mg and Cu-Mg-Ce alloys with 60% cold deformation aged at 420 °C: (a) hardness; (b) electrical conductivity

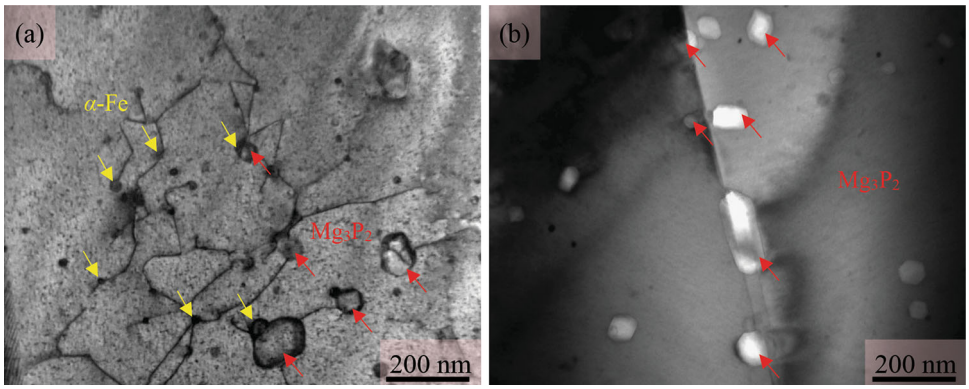

Fig. 8 (a) and (b) TEM images of the Cu-Mg-Ce alloy with 60% cold deformation aged at 480 °C for 480 min

electrons in the matrix, which improved the electrical conductivity of the Cu-Mg-Ce alloy.

4.2 Effects of the Mg_3P_2 Phase on the Cu-Mg-Ce Alloy

As mentioned above, the precipitates are pinning dislocations and twin boundaries, which prevent the dynamic recrystallization in the aging process. In order to identify the type of the particle, TEM images of the Cu-Mg-Ce alloy aged at a higher temperature are obtained in Fig. 6. At this condition, particles with larger size are easier to distinguish. Figure 8 shows the TEM images of the Cu-Mg-Ce alloy with 60% cold deformation aged at 480 °C for 480 min. As shown in Fig. 8(a), both α-Fe and Mg_3P_2 pinned dislocations. However, in Fig. 8(b), only Mg_3P_2 particles were observed in the grain boundaries to resist grain boundaries motion in the long-time aging process. On the contrary, no α-Fe particles appeared in the grain boundaries. Besides, the matrix around the Mg_3P_2 phase is relatively pure, and there is almost no dislocation entanglement. It is noteworthy that in Fig. 8(a), the larger α-Fe particles pin the dislocations, hindering the movement of dislocations. The smaller particles are dispersed in the matrix and caused dispersion strengthening. This indicates that α-Fe particles have little effects on pinning grain boundaries. Therefore, it can be inferred that the main phase of dispersion strengthening during aging is α-Fe. Combined with the above discussion, it can be concluded that the appearance of the α-Fe and Mg_3P_2 particles inhibits the movement of dislocations. Meanwhile, Mg_3P_2 particles play an important role in hindering the occurrence of dynamic recrystallization during aging by pinning the motion of grain boundaries.

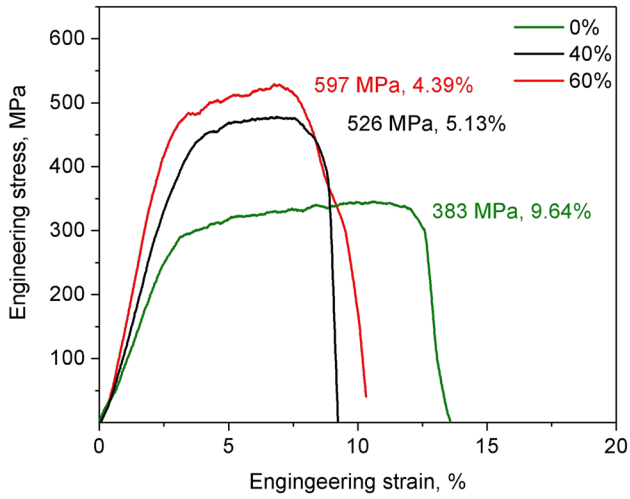

Fig. 9 Tensile properties of the Cu-Mg-Ce alloy aged at 420 °C for 20 min with various cold deformations

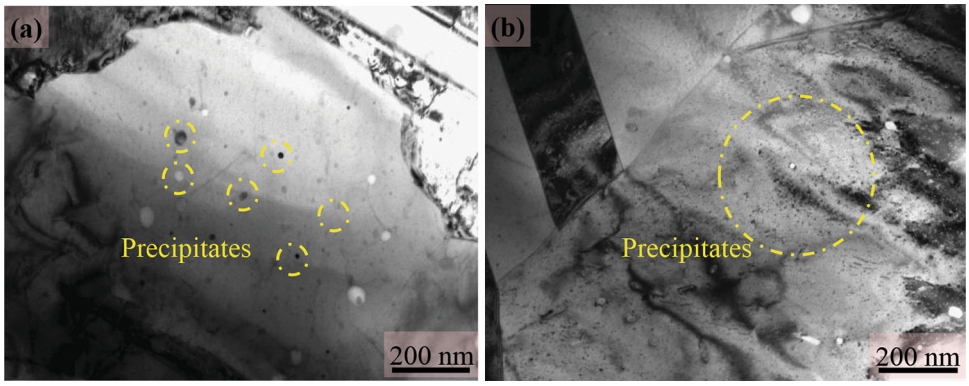

Fig. 10 TEM images of the Cu-Mg-Ce alloy aged at 420 °C for 20 min with various cold deformations (a) 40%; (b) 60%

4.3 Effects of Dislocations on the Precipitation Behavior

It has been mentioned that Cu-Mg-Ce alloy with 60% cold deformation shows the peak hardness after aging at 420 °C for 20 min. In order to investigate the effects of dislocations on the precipitation behavior, the corresponding Engineering stress–strain curves of the Cu-Mg-Ce alloy at this aging condition with 0, 40 and 60% cold deformation are shown in Fig. 9.

The specimen with 60% cold deformation exhibits the highest ultimate tensile strength of 597 MPa and the elongation of 4.39%. The reason is that cold deformation before aging treatment contributes to the precipitation of the secondary phase. The larger deformation caused more vacancies and deformation dislocations in the alloy matrix. Sengupta et al. (Ref 38) found the "strain-induced precipitation" in copper-base age-hardenable alloy. The main reason of strain promoting the precipitation behavior of microalloyed elements is that deformation leads to a large number of dislocations. Dislocations not only provide a fast channel for the diffusion of microalloyed elements, but also promote the nucleation of precipitates in many ways, such as producing a large number of deformation bands, which compensates for the strain energy required for nucleation. In these parts, the energy required for nucleation of precipitates is small, the nucleation position is increased, and the nucleation capacity is relatively large. At the same time, the deformation will press the grains of the sample into strips, increase the area of the grain boundary greatly, compensate the interface energy needed for nucleation, and the grain boundary is the best position for particle precipitation, and the deformation can promote the precipitation of microalloyed elements. Figure 10(a) and (b) show the TEM images of the Cu-Mg-Ce alloy aged at 420 °C for 20 min with 40 and 60% cold deformation, respectively. The smaller and more evenly distributed secondary phase (marked by the circle) appears in the matrix with 60% cold deformation. Besides, it can be seen clearly that the number of secondary phases in the alloy after 60% cold deformation is obviously more than that after 40% cold deformation, which leads to higher distortion energy storage, faster precipitation of the secondary phase and larger volume fraction. During the aging process, the dislocation density decreased gradually and the dislocation strengthening effect decreased. The cold deformation process before aging changes the aging precipitation behavior of the alloy, accelerates the aging process and improves the strength and hardness of the alloy.

5. Conclusions

Aging treatment of the Cu-Mg-Ce alloy after various cold deformations was conducted at the aging temperature ranging from 400 to 480 °C and the aging time ranging from 10 to 480 min. The properties and phase analysis of the Cu-Mg-Ce alloy were discussed. The main conclusions are summarized as follows:

(1) Cu-Mg-Ce alloy has the maximum hardness aging at 420 °C. Due to the growth of secondary phase at a higher temperature, an obvious over-aging phenomenon occurs when the temperature is higher than 420 °C.
(2) The occurrence of the peak-aging stage (420 °C and 20 min) in the aging process is attributed to the precipitation of ultrafine secondary phases.
(3) The addition of Ce promoted the precipitation of the secondary phases, which improved the hardness and electrical conductivity of the Cu-Mg alloy. The nanoscale α-Fe and Mg_3P_2 secondary phases, pinned at dislocations and twin boundaries, improved the softening resistance of the Cu-Mg-Ce alloy.
(4) The Mg_3P_2 particles play an important role in hindering the occurrence of dynamic recrystallization during aging by pinning the motion of grain boundaries. Furthermore, the appearance of Mg_3P_2 hindered the coarse Fe_2P or Fe_3P phases and increased the electrical conductivity of the Cu-Mg-Ce alloy.
(5) Optimal aging parameters for the Cu-Mg-Ce alloy are 60% cold deformation aged at 420 °C for 20 min with the hardness of 205.82 HV, the electrical conductivity of 73.59%IACS, the ultimate tensile strength of 597 MPa, and the elongation of 4.39%. Compared with the Cu-Mg alloy, Ce addition enhanced the hardness and electrical conductivity by 22 and 9%, respectively.

Acknowledgments

This work was supported by the National Natural Science Foundation of China (U1704143), the Open Cooperation Project of Science and Technology of the Hennan Province (172106000058 and 182106000018), and by the National Science Foundation (IRES 1358088).

References

1. N. Takata, S.H. Lee, and N. Tsuji, Ultrafine Grained Copper Alloy Sheets Having Both High Strength and High Electric Conductivity, *Mater. Lett.*, 2009, **63**, p 1757–1760
2. T.S. Srivatsan, N. Narendra, and J.D. Troxell, Tensile Deformation and Fracture Behavior of an Oxide Dispersion Strengthened Copper Alloy, *Mater. Des.*, 2000, **21**, p 191–198
3. H.H. Li, S.H. Zhang, Y. Chen, M. Cheng, H.W. Song, and J.S. Liu, Effects of Small Amount Addition of Rare Earth Ce on Microstructure and Properties of Cast Pure Copper, *J. Mater. Eng. Perform.*, 2015, **8**, p 2857–2865
4. C.C. Zhu, A.B. Ma, J.H. Jiang, X.B. Li, D. Song, D.H. Yang, and J.Q. Chen, Effect of ECAP Combined Cold Working on Mechanical Properties and Electrical Conductivity of Conform-Produced Cu–Mg Alloys, *J. Alloys Compd.*, 2014, **582**, p 135–140
5. G. Zhen, Y. Kim, L.H. Chuang, J.M. Koo, C.S. Seok, K. Lee, and S.Y. Kwon, Bending Fatigue Life Evaluation of Cu–Mg Alloy Contact Wire, *Int. J. Precis. Eng. Man.*, 2014, **15**, p 1331–1335
6. K. Abib, J.A.M. Balanos, B. Alili, and D. Bradai, On the Microstructure and Texture of Cu–Cr–Zr Alloy After Severe Plastic Deformation by ECAP, *Mater. Charact.*, 2016, **112**, p 252–258
7. L.X. Sun, N.R. Tai, and K. Lu, A High Strength and High Electrical Conductivity Bulk Cu–Cr–Zr Alloy with Nanotwins, *Scr. Mater.*, 2015, **99**, p 73–76
8. C. Watanabe and R. Monzen, Coarsening of δ-Ni_2Si Precipitates in a Cu–Ni–Si Alloy, *J. Mater. Sci.*, 2011, **46**, p 4327–4335
9. X.Z. Chen, Y.Z. Yang, Q.S. Lin, and X.J. Bai, The Optimization of Thermomechanical Treatment and Properties of Cu–Fe–P Alloy C194, *Adv. Mater. Res.*, 2012, **415–417**, p 724–727
10. S.G. Mu, F.A. Guo, Y.Q. Tang, X.M. Cao, and M.T. Tang, Study on the Microstructure and Properties of Aged Cu–Cr–Zr–Mg–RE Alloy, *Mater. Sci. Eng. A*, 2008, **475**, p 235–240
11. S. Lee, H. Matsunaga, X. Sauvage, and Z. Horita, Strengthening of Cu–Ni–Si Alloy Using High-Pressure Torsion and Aging, *Mater. Charact.*, 2014, **90**, p 62–70
12. P. Liu, B.X. Kang, X.G. Cao, J.L. Huang, B. Yen, and H.C. Gu, Aging Precipitation and Recrystallization of Rapidly Solidified Cu–Cr–Zr–Mg Alloy, *Mater. Sci. Eng. A*, 1999, **265**, p 262–267
13. F.A. Guo, C.J. Xiang, C.X. Yang, X.M. Cao, and Y.Q. Tang, Study of Rare Earth Elements on the Physical and Mechanical Properties of a Cu–Fe–P–Cr Alloy, *Mater. Sci. Eng. B*, 2008, **147**, p 1–6
14. B.J. Wang, Y. Zhang, B.H. Tian, V. Yakubov, J.C. An, and A.A. Volinsky, Effects of Ce and Y Addition on Microstructure Evolution and Precipitation of Cu–Mg Alloy During Hot Deformation, *J. Alloys Compd.*, 2019, **781**, p 118–130
15. X.L. Lu, F. Chen, W.S. Li, and Y.F. Zheng, Effect of Ce Addition on the Microstructure and Damping Properties of Cu–Al–Mn Shape Memory Alloys, *J. Alloys Compd.*, 2009, **480**, p 608–611
16. Y. Zhang, A.A. Volinsky, H.T. Tran, Z. Chai, P. Liu, B.H. Tian, and Y. Liu, Aging Behavior and Precipitates Analysis of the Cu–Cr–Zr–Ce Alloy, *Mater. Sci. Eng. A*, 2016, **650**, p 248–253
17. T. Shibayanagi, K. Takada, K. Matsumoto, and Y. Umakoshi, Effect of Secondary Phase on Grain Growth Process of α/β Dual-Phase CuZn Alloy, *Scr. Mater.*, 1997, **37**, p 667–672
18. Q. Lei, Z. Li, M.P. Wang, L. Zhang, Z. Xiao, and Y.L. Jia, The Evolution of Microstructure in Cu–8.0Ni–1.8Si–0.15Mg Alloy During Aging, *Mater. Sci. Eng. A*, 2010, **527**, p 6728–6733
19. Y. Zhang, B.H. Tian, A.A. Volinsky, H.L. Sun, Z. Chai, P. Liu, X.H. Chen, and Y. Liu, Microstructure and Precipitate's Characterization of the Cu–Ni–Si–P Alloy, *J. Mater. Eng. Perform.*, 2016, **25**, p 1336–1341
20. J.Y. Cheng, B. Shen, and F.X. Yu, Precipitation in a Cu–Cr–Zr–Mg Alloy During Aging, *Mater. Charact.*, 2013, **81**, p 68–75
21. H. Conrad and J. Narayan, On the Grain Size Softening in Nanocrystalline Materials, *Scr. Mater.*, 2000, **42**, p 1025–1030
22. N.M. Heckman, M.F. Berwind, C. Eberl, and A.M. Hodge, Microstructural Deformation in Fatigued Nanotwinned Copper Alloys, *Acta Mater.*, 2018, **144**, p 138–144
23. P. Coddet, C. Verdy, C. Coddet, and F. Debray, Effect of Cold Work, Second Phase Precipitation and Heat Treatments on the Mechanical Properties of Copper–Silver Alloys Manufactured by Cold Spray, *Mater. Sci. Eng. A*, 2015, **637**, p 40–47
24. I.S. Batra, G.K. Dey, U.D. Kulkarni, and S. Banerjee, Precipitation in a Cu–Cr–Zr Alloy, *Mater. Sci. Eng. A*, 2003, **356**, p 32–36
25. H.E. Mofrad, S. Raygan, B.A. Forghani, K. Hanaei, and F.K. Ahadi, Effect of Cold-Working and Aging Processes on the Microstructure, Mechanical Properties and Electrical Conductivity of Cu–13.5%Mn–4%Ni–1.2%Ti Alloy, *Mater. Des.*, 2012, **41**, p 182–194
26. A.P. Zhilyaev, I. Shakhova, A. Morozova, and R. Kaibyshev, Grain Refinement Kinetics and Strengthening Mechanisms in Cu–0.3Cr–0.5Zr Alloy Subjected to Intense Plastic Deformation, *Mater. Sci. Eng. A*, 2016, **654**, p 131–142
27. K.X. Wei, W. Wei, F. Wang, Q.B. Du, IV, and JHu Alesandrov, Microstructure, Mechanical Properties and Electrical Conductivity of Industrial Cu–0.5%Cr Alloy Processed by Severe Plastic Deformation, *Mater. Sci. Eng. A*, 2011, **528**, p 1478–1484
28. B.J. Wang, Y. Zhang, B.H. Tian, J.C. An, A.A. Volinsky, H.L. Sun, Y. Liu, and K.X. Song, Effects of Ce Addition on the Cu–Mg–Fe Alloy Hot Deformation Behavior, *Vacuum*, 2018, **155**, p 594–603
29. H.G. Kim, T.W. Lee, S.Z. Han, K.J. Euh, W.Y. Kim, and S.H. Lim, Microstructural Study on Effects of C-Alloying on Cu–Fe–P Cast Alloy, *Met. Mater. Int.*, 2012, **18**, p 335–339
30. L.Q. Gao, X. Yang, X.F. Zhang, Y. Zhang, and H.L. Sun, Aging Behavior and Phase Transformation of the Cu–0.2 wt%Zr–0.15 wt%Y Alloy, *Vacuum*, 2019, **159**, p 367–373
31. C.D. Xia, Y.L. Jia, W. Zhang, K. Zhang, Q.Y. Dong, G.Y. Xu, and M.P. Wang, Study of Deformation and Aging Behaviors of a Hot Rolled-Quenched Cu–Cr–Zr–Mg–Si Alloy During Thermomechanical Treatments, *Mater. Des.*, 2012, **39**, p 404–409
32. M. Avrami, Granulation, Phase Change, and Microstructure Kinetics of Phase Change. III, *J. Chem. Phys.*, 1941, **9**, p 177–184
33. N. Stanford, D. Atwell, A. Beer, C. Davies, and M.R. Bamett, Effect of Microalloying with Rare-Earth Elements on the Texture of Extruded Magnesium-Based Alloys, *Scr. Mater.*, 2008, **59**, p 772–775
34. D. Janovszky, K. Tomolya, M. Sveda, A. Sycheva, and G. Kaptay, Effect of Y and Ni Addition on Liquid Immiscibility in Cu–Zr–Ag Ternary Alloys, *J. Alloys Compd.*, 2014, **615**, p S616–S620
35. A. Rohatgi, K.S. Vecchio, and G.T. Gray, The Influence of Stacking Fault Energy on the Mechanical Behavior of Cu and Cu–Al Alloys: Deformation Twinning, Work Hardening, and Dynamic Recovery, *Metall. Mater. Trans. A*, 2001, **32**, p 135–145
36. G.W. Peng, X.P. Gan, Y.X. Jiang, Z. Li, and K.C. Zhou, Effect of Dynamic Strain Aging on the Deformation Behavior and Microstructure of Cu–15Ni–8Sn Alloy, *J. Alloys Compd.*, 2017, **718**, p 182–187
37. A.K. Shukla, S.V.S. Narayana Murty, S.C. Sharma, and K. Mondal, Aging Behavior and Microstructural Stability of a Cu–8Cr–4Nb Alloy, *J. Alloys Compd.*, 2014, **590**, p 514–525
38. P.K. Sengupta and J. Rezek, Microstructural Refinement of a Copper-Base Age-Hardenable Alloy Through Thermomechanical Processing, *J. Mater. Sci. Lett.*, 1986, **5**, p 445–449